



New Highly Stable Ionic Compounds Composed of Multivalent Graphene Quantum Dot Anions and Alkali Metal Cations

Hong Chul Lim^{+, [a, b]} Min-Cheol Kim^{+, [c, d]} Ayoung Kim,^[e] Eunji Park,^[a] Yunjae Park,^[f] Rakwoo Chang,^[g] Jong-In Hong,^[h] Kyung-Won Park,^{*[c]} Ik-Soo Shin,^{*[a]} and Hansu Kim^{*[e]}

Developing electrolytes with new chemical structures that simultaneously satisfy excellent ionic conductivity, chemical stability, and thermal stability is an indispensable prerequisite for studying next-generation electrochemical. Herein, we propose a new class of ionic compounds consisting of graphene quantum dots (GQD) polyanions with alkali metal cations. The synthesized solid salts readily dissolve in various solvents ranging from water to carbonates allowing highly conductive liquid electrolytes for electrochemical systems. Molecular dynamics simulation with the electrochemical characterization reveals that the ionic compounds provide highly abundant free metal cations with highly stable GQD polyanions, and negligible ion pairs in solution. The lithium salt (Li-GQD) shows higher

lithium transference number than the conventional LiPF₆ electrolyte, which improves the interfacial stability of Li metals and leads to a decrease in overvoltage at a high C-rate in battery performance. The Li-GQD electrolyte solution offers a wide electrochemical window of -0.2–5 V, which can reliably apply to various electrode materials (graphite, Li₄Ti₅O₁₂, and LiCoO₂). Prussian blue thin film utilizing K-GQD as electrolyte shows significantly improved electrochromic behaviour and higher K⁺ cation mobility than other controls using conventional electrolytes. We expect our study on the GQD ionic complex to be another signpost for exploring an innovative electrolyte for electrochemical devices.

Introduction

An electrolyte salt generally refers to a substance that promotes electrical conductivity by transporting ions to a medium in the form of a dissolved mixture.^[1–3] It is omnipresent in many parts of our daily lives, ranging from natural systems, such as homeostasis in our bodies, to manufactured products like batteries.^[4,5] For example, sodium chloride (NaCl) dissociates into Na⁺ and Cl⁻ ions, which play a pivotal role in regulating blood pressure, controlling fluid balance, and maintaining conditions suitable for muscle and nerve functions.^[6,7] The aqueous solution of NaCl, brine, was also

employed as an electrolyte solution by Alessandro Volta, who invented the battery. Ammonium chloride (NH₄Cl) has been widely used as a high nitrogen fertilizer in agriculture, and it has also been utilized as an electrolyte in zinc-carbon batteries.^[8,9] Thus, electrolyte salt is a critical component in electrochemical applications, such as rechargeable batteries, electrochemical capacitors, electrolysis devices, and fuel cells that convert (or store) chemical energy into electrical energy.^[10–12] Over the past decades, research has been actively conducted to develop an electrolyte salt that provides excellent ionic conductivity, chemical stability, and thermal stability in various applications.^[13,14] Research efforts have been mainly

[a] H. Chul Lim,⁺ E. Park, Prof. I.-S. Shin

Department of Chemistry
Soongsil University
Seoul, 06978, Republic of Korea
E-mail: extant@ssu.ac.kr
eun_ji904@naver.com

[b] H. Chul Lim⁺
Present Address:
Department of Fine Chemical New Material
Sangji University
Wonju, 26339, Republic of Korea

[c] M.-C. Kim,⁺ Prof. K.-W. Park
Department of Chemical Engineering
Soongsil University
Seoul, 06978, Republic of Korea

E-mail: kwpark@ssu.ac.kr
[d] M.-C. Kim⁺
Present Address:
Division of Physics and Semiconductor Science
Dongguk University
Seoul, 04620, Republic of Korea

[e] A. Kim, Prof. H. Kim
Department of Energy Engineering
Hanyang University
Seoul, 04763, Republic of Korea
E-mail: khansu@hanyang.ac.kr

[f] Y. Park
Department of Chemistry
Kwangwoon University
Seoul, 01897, Republic of Korea

[g] Prof. R. Chang
Department of Applied Chemistry
University of Seoul
Seoul, 02504, Republic of Korea

[h] Prof. J.-I. Hong
Department of Chemistry
Seoul National University
Seoul, 08826, Republic of Korea

[+] These authors contributed equally to this work.

Supporting information for this article is available on the WWW under <https://doi.org/10.1002/batt.202100337>

focused on devising a new type of anions that offer acceptable solubility and chemical inertness to ionic salt. Unfortunately, only a few candidates, such as hexafluorophosphate (PF_6^-), tetrafluoroborate (BF_4^-), triflate ($\text{OSO}_2\text{CF}_3^-$), and perchlorate (ClO_4^-), have been, to a limited extent, commercialized so far. Ionic liquid or inorganic solid-based electrolytes have also been investigated because they provide mechanical flexibility and safety benefits. Still, their commercialization has been hampered by low ionic conductivity and high interfacial resistance.^[15–18]

We report a new class of ionic compounds composed of multivalent graphene quantum dot (GQD) polyanions and their equivalent alkali cations such as Li^+ , Na^+ , and K^+ . GQDs with similar photophysical properties as metallic quantum dots have been studied mainly in bio-imaging and light-emitting diode as fluorescent nanomaterial.^[19–21] Herein, we have rather focused on the chemical properties, such as the carbonized structure of GQD and oxygen-containing functional branches.^[22] We anticipated that the former could provide enough material durability to withstand harsh electrochemical environments when dissociated in a solvent to become polyanions. The latter allows the formation of electrolyte salts through ionic bonds with alkali cations and also yields high ionic dissociation due to the bulky anionic structure. The ionic complexes based on the GQD polyanion were synthesized via a two-step fabrication process; first, the hydrothermal oxidation of carbon nanofibers results in 6 nm-sized GQD with sp^2/sp^3 hybridized carbon structure in the core and hydroxyl and carboxylic groups on the edges. Then,

the carboxylate anions ($-\text{COO}^-$) at the edge of GQD yielded a soluble ionic complex such as Li-GQD, Na-GQD, and K-GQD through electrostatic attraction with alkali metal cations such as Li^+ , Na^+ , and K^+ (Figure 1a). The synthesized ionic complexes exhibited low Coulombic energy, excellent thermal/electrochemical inertness, and decent ionic conductivity dissolved in aqueous and organic solvents. Molecular dynamics (MD) simulation revealed that the Li-GQD solution is thermodynamically more stable than the LiPF_6 solution, suggesting that ionic complexes based on GQD polyanions provide high cationic dissociation in the dissolved state. Electrochemical impedance spectroscopy (EIS) and DC polarization experiments confirmed that the lithium transference number (t_{Li}^+) showed a very high level (0.85) in the Li-GQD solution, allowing stable operation of Li stripping and plating test up to 200 h. We also confirmed that the electrochemical stability window of Li-GQD is wide enough to be used in several representative electrode materials of lithium-ion batteries (LIBs), such as graphite (0.05–1.5 V vs. Li/Li^+), $\text{Li}_4\text{Ti}_5\text{O}_{12}$ (1.0–3.0 V vs. Li/Li^+), and LiCoO_2 (3.5–4.3 V vs. Li/Li^+). In a comparative study with conventional aqueous electrolytes, Prussian blue ($\text{KFe}^{III}[\text{Fe}^{II}(\text{CN})_6]$, PB) exhibited superior electrochromic performance of better colouration efficiency, higher optical contrast and excellent cycling performance in the K-GQD electrolyte.

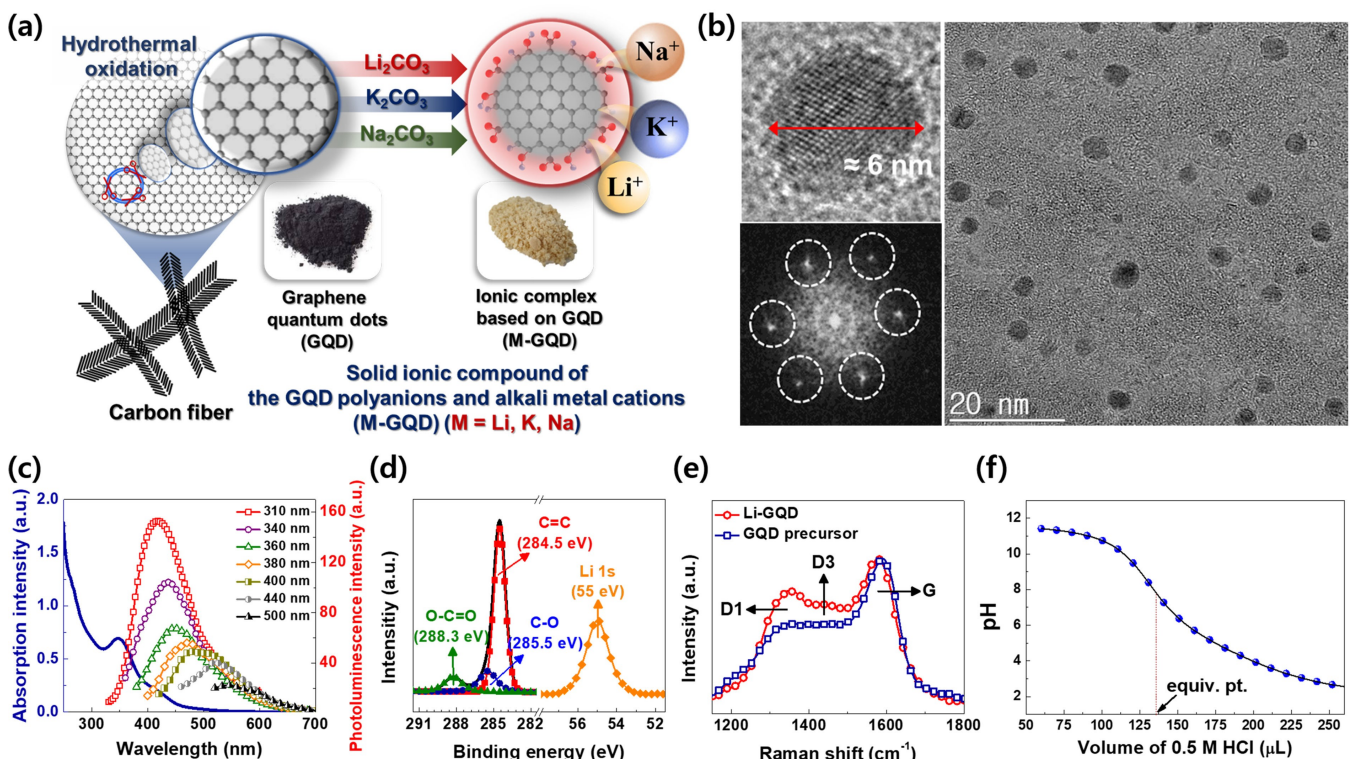


Figure 1. a) Schematic for preparation of the ionic complexes. b) HRTEM and its corresponding fast Fourier transform (FFT) pattern. c) UV-vis absorption and photoluminescence spectra. d) XPS spectra of the prepared Li-GQD. e) Raman spectra (closed rectangle: pristine GQD precursor and open circle: Li-GQD). f) Acid-base titration curve of the 10 mL aqueous Li-GQD solution (1 mg mL⁻¹) with the 0.5 M HCl titrant.

Results and Discussion

Characteristics of ionic complexes based on the GQD polyanion

The elemental content and size distribution in the ionic compounds, including alkali metal cations and the GQD polyanion, is hard to control precisely. However, to obtain an ionic compound with constant chemical composition and narrow size distribution, we carried out strict separation processes of several steps of centrifugation and dialysis,^[23] resulting in Li-GQD with an average diameter of 6 nm (see the experimental procedures). The high-resolution transmission electron microscopy (HRTEM) images in Figure 1(b) showed that Li-GQD, having a circular or elliptical shape of ~6 nm diameter, exhibited the sp^2 conjugated carbon networks in the core together with an amorphous structure on edge. Note that the Li^+ counter cations presumably existing as the form of $-COO^-Li^+$ on the peripheral branches are inherently invisible.^[24,25] Two absorption peaks around 269 and 347 nm were observed in the UV-vis spectrum where the former corresponds to the $\pi-\pi^*$ transition of the sp^2 hybridization of C=C at the core, and the latter is attributed to the n- π^* transition associated with C=O or C–O bond on edge (Figure 1c).^[26,27] Li-GQD showed excitation-dependent fluorescence, which is identical to that of the GQD precursor. The emission peak shifted toward a long wavelength as the excitation energy decreased. The blue emission originates from the quantum confinement of the sp^2 carbon in the core, and the redshift is attributed to the oxygen functional groups on edge. The sp^2 carbons showed a prominent peak around 284.5 eV with the other two peaks associated with the C–O (285.5 eV) and O=C=O (288.3 eV) groups in the X-ray photoelectron spectroscopy (XPS) (Figure 1d).^[28] The presence of the Li element was clearly observed at the peak of ~55.0 eV, and the atomic ratios of the elements carbon, oxygen, and lithium in Li-GQD calculated by XPS spectrum are 71%–74%, 18%–22%, and 5%–6%, respectively. Raman spectroscopy showed the G- and D-band peaks, indicating the sp^2 and amorphous carbons in Li-GQD and the GQD precursor, respectively (Figure 1e). While that of the GQD precursor appeared at 1576 cm⁻¹, the G-band peak in Li-GQD was found at 1593 cm⁻¹. This is due to mass increasing by the electrostatic binding of the Li^+ cations to the GQD polyanion.^[29–31] As a result, the Li-GQD can be determined as the ionic complex consisting of several Li^+ cations and one GQD polyanion through electrostatic attraction. In thermal gravimetric analysis (TGA), Li-GQD showed high thermal stability with no particular change under heating conditions above 550 °C. From 568 °C, a gentle weight reduction has since begun, reaching a decrease of about 5% at 655 °C (Figure S1).

The number of moles of Li^+ per 1 mg of Li-GQD can be estimated in three ways. In the XPS data, it is calculated from 3.92 (in the empirical formula of $C_{74}O_{22}Li_5$) to 5.08 $\mu\text{mol mg}^{-1}$ ($C_{71}O_{18}Li_6$) under ignoring the contribution of hydrogen. On the other hand, in the acid-base titration experiment (Figure 1f), the endpoint, measured by adding the 0.5 M HCl titrant to the 10 mL aqueous solution of Li-GQD (1 mg mL⁻¹) was 136.5 μL .

Assuming that all the carboxylate at the Li-GQD periphery exists in the ionic form with Li^+ , the maximum number of moles of Li^+ is calculated as 6.85 μmol per 1 mg of Li-GQD same as the number of the calculated carboxylate. From the pH value of the half endpoint, pK_a of -COOH can be calculated as 2.27 which is under the range of the carboxylic acid derivatives. In addition, it also be estimated as 7.85 $\mu\text{mol mg}^{-1}$ through the ICP-MS analysis. The deviation in the molar number of Li^+ cation per 1 mg of Li-GQD can be varied between XPS, acid-base titration, and the ICP-MS analysis because of the methodological difference.

Molecular dynamics simulation and characterization of the Li-GQD electrolyte

To understand the thermodynamic behaviour for Li-GQD in terms of molecular scale, molecular dynamics simulation (MD) was conducted. A GQD polyanion was modelled as a 4×4 hexagonal fragment functionalized with 3 hydroxyl (-OH) of the phenol and 6 carboxylate (-COO⁻) groups of the benzoic acid structure at the edge (Figure S2). Only -COO⁻ was considered the anionic functional group that can only form ionic interaction with Li^+ because the titration curve of the hydroxyl group was barely observed in the acid-base titration of Li-GQD (Figure 1f). The six Li^+ cations, initially placed randomly in the simulation box, were quickly adsorbed on the carboxylate groups. The aggregation of the GQD polyanions was not observed during the equilibrium MD simulation (Figure 2a). It implies that $Li_6(GQD)$ system is significantly stable, which is in stark contrast with the $LiPF_6$ system reported to tend to be aggregated irreversibly under the same Li^+ cations concentration.^[32,33] To understand the affinity between the anions and cations in the ionic complex systems, we have calculated the radial distribution function, $g_{AB}(r)$, between ions A and B,^[34] which is defined as Equation (1):

$$g_{AB}(r) = \frac{V}{N_A N_B} \langle \sum_{i=1}^{N_A} \sum_{j=1}^{N_B} \delta(\mathbf{r} - \mathbf{r}_{ij}) \rangle \quad (1)$$

where V is the system volume, N_A and N_B are respectively the numbers of ions A and B, r_{ij} is the vector connecting the COM of the i -th molecule of ion A and the COM of the j -th molecule of ion B, $\delta(\dots)$ and $\langle \dots \rangle$ correspond to the delta function and the ensemble average, respectively.

The time evolutions of $g_{Li^+GQD^-}(r)$ and $g_{GQD,GQD}(r)$ developed a strong double peak around 8 and 9 Å in a very short simulation time, which indicates that Li^+ cations are strongly attached to the carboxylate groups of GQD (Figure 2b and c). On the other hand, $g_{GQD,GQD}(r)$ displayed a broad peak between 10–20 Å. This implies that the attraction between GQD polyanions is weak, resulting in acting of the attraction and repulsion between the GQD polyanions repeatedly, as discussed above. To quantify the binding free energy between the two GQD polyanions, we have employed the umbrella sampling method. The binding free energy of the GQD

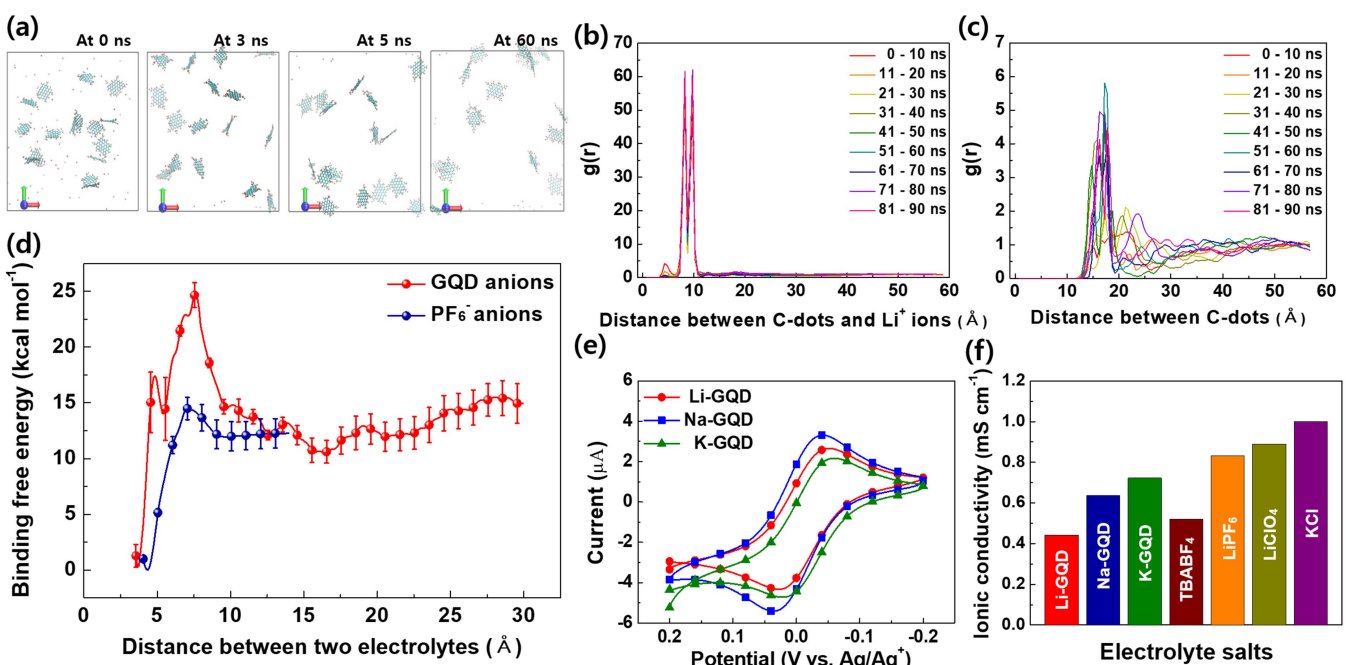


Figure 2. a) Molecular model of the snapshots of the time evolution of the bulk Li₆GQD system with [Li⁺] = 100 mM. The radial distribution functions of b) $g_{\text{Li}^+\text{GQD}^-}(r)$ and c) $g_{\text{GQD,GQD}}(r)$. d) Binding free energy between two GQD ions along with that between two PF₆⁻ ions. e) Cyclic voltammograms of 1 mM ferrocene according to the 0.1 M M-GQD electrolyte solution [MeOH:H₂O (3:1 v/v)]. (Li-GQD: red line with closed circle, Na-GQD: blue line with closed rectangle, and K-GQD: green line with closed triangle). f) Ionic conductivities of various electrolyte solutions.

polyanions showed a strong repulsive peak of ~9.5 kcal mol⁻¹ around 7.6 Å, which separated a deeply attractive region of ~14.7 kcal mol⁻¹ around 3.6 Å from a shallow and broad attractive region around 9.4–26.7 Å (Figure 2d).

This behavior is similar to the potential energy between charged colloids with electric double layers in the Derjaguin-Landau-Verwey-Overbeek (DLVO) theory.^[35] According to the DLVO theory, the van der Waals attraction is compensated for by the electrostatic repulsion between electric double layers. In the case of charged colloids, the particles aggregation arising from the stabilizing effect of the shallow minimum is called flocculation; on the other hand, the irreversible aggregation of individual particles to large particles, called coagulation, occurred when the separation of the particles was so small that the van der Waals attraction became dominant. In the case of the GQD polyanions, the strong repulsive free energy seems to be originated from the energetic penalty required to remove the solvent molecules intercalated between the planar regions of the GQD polyanions (Figure S2). Because of the high free energy barrier, the undesirable coagulation of the GQD polyanions mediated by Li⁺ cations would be easily avoided. This is in stark contrast with the PF₆⁻ anion system, the free energy of which is also shown in Figure 2(d). In the case of the PF₆⁻ anions, the repulsive free energy barrier was as low as 2 kcal mol⁻¹, which can be easily overcome by thermal energy. As a result, ionic complexes based on the GQD polyanion are expected to provide free Li⁺ cations and the GQD polyanions because they are stably distributed in the dissolved state.

To experimentally verify the simulation results, we dissolved the M-GQD ionic complexes (M=Li, Na, K) in mixed solvents

(MeOH:H₂O 3:1 v/v) and evaluated their properties as the supporting electrolyte compared with commercially available salts, such as LiPF₆, LiClO₄, TBABF₄, and KCl. Ferrocene (C₁₀H₁₀Fc, Fc), a representative electroactive species, successfully exhibited quasi-reversible, one-electron oxidation in the electrolyte solutions, which implies that the GQD polyanion is electrochemically inert with no interference to the redox processes of the Fc (Figure 2e and Table S1). Interestingly, the observed diffusion coefficient (D_0) of Fc and the solution viscosity (η) was clearly divided into ionic complexes based on the GQD polyanion and the control groups (Figure S3). We think this is due to the size effect of the nano-scaled GQD polyanion compared to the single molecule-based control groups.^[36] Na-GQD and K-GQD showed a slightly lower ionic conductivity than the control groups despite the solution viscosities of M-GQDs were about 2 times as high (Figure 2f). This is probably due to the weak ion association of the GQD polyanion and the counter cations, resulting in more free ions in the dissolved state. The order of ionic conductivity increases to Li-GQD < Na-GQD < K-GQD due to the ionic dissociation according to the cation size and the viscosity relating to the hydrated ion size (Figure 2f).^[37,38]

Electrochemical properties of LIBs based on Li-GQD

Weakly coordinating anions (WCAs) with relatively large molecular size and charge delocalization provide lower ionization energy with cations in ionic salt than conventional anions (PF₆⁻, BF₄⁻, ClO₄⁻) so that they are generally expected to offer

higher cation transference numbers.^[39–42] MD simulation results and electrochemical properties of Li-GQD conducted in the previous part show that Li-GQD meets the properties of WCA. To confirm the feasibility of Li-GQD as an electrolyte salt for LIBs, we carried out the electrochemical battery study, including voltammetry, lithium stripping and plating experiments, and cell tests using various electrode materials. The Li-GQD electrolyte mixture was prepared using 331.2 mg of Li-GQD dissolved in the 100 mL (26 mM) of ethylene carbonate:dimethyl carbonate (1:1 v/v%). LiPF₆ (26 mM) dissolved in the same solvent was prepared as a control group (Control). Although Li-GQD is highly soluble in protic solvents, yet it exhibits relatively poor solubility in aprotic organic solvents, so that we set the concentration of all electrolytes to 26 mM.

Cyclic voltammograms (CV) were measured to evaluate the electrochemical stability of the battery cells consisting of a polypropylene separator between a Li metal and a Pt disk electrode as the working electrode. In Figure 3(a), the Li-GQD electrolyte begins to decompose above 4.5 V, which is the cut-off voltage of most electrode materials used for LIB. The Li-GQD electrolyte is considered electrochemically stable under the cut-off condition of LIB. The small redox peaks at –0.2–5.0 V (vs. Li/Li⁺) are caused by the Li–Pt alloying and de-alloying reactions.^[43] EIS and the DC polarization measurement provide the ionic conductivity and lithium transference number (t_{Li^+}) of the Li-GQD electrolyte (Figures S4 and S5). The ionic conductiv-

ity of the Li-GQD electrolyte and Control measured at 30 °C were 6.85×10^{-2} and 24.2×10^{-2} mS cm⁻¹ respectively. In addition, under various temperatures (30–70 °C), the ionic conductivity of the Li-GQD electrolyte was lower than that of Control. The ionic radius of the GQD polyanion is significantly larger than that of the PF₆[–] anion (0.245 nm)^[44,45] allowing slower ionic mobility of the GQD polyanion, which presumably results in lower conductivity to Control.^[46] However, t_{Li^+} of the Li-GQD electrolyte (0.85) was much higher than Control (0.63), which approaches that of a single Li⁺ cation conductor (Figure 3b). This correlates with the large and heavy molecular structure of the GQD polyanion and the high abundance of free Li⁺ cations from the simulation study. Electrolytes with high t_{Li^+} values are known to reduce the ion concentration gradient at the electrode-electrolyte interface and affect the lithium dendrite formation process during cell testing.^[47–49] In lithium stripping and plating tests (Figure 3c), the polarization of the Li-GQD electrolyte increased by only 23.8% from 20.1 mV at the initial cycle to 24.9 mV after 200 hr (a current density of 0.1 mA cm⁻²). On the other hand, the polarization of Control changed from 27.5 mV to 50.6 mV with an almost double increase. This indicates that the Li-GQD electrolyte can effectively stabilize the lithium stripping and plating process compared to Control and inhibit lithium dendrite growth.^[47]

Coin cell performances using three representative electrode materials: graphite, Li₄Ti₅O₁₂ (LTO), and LiCoO₂ (LCO) indicate

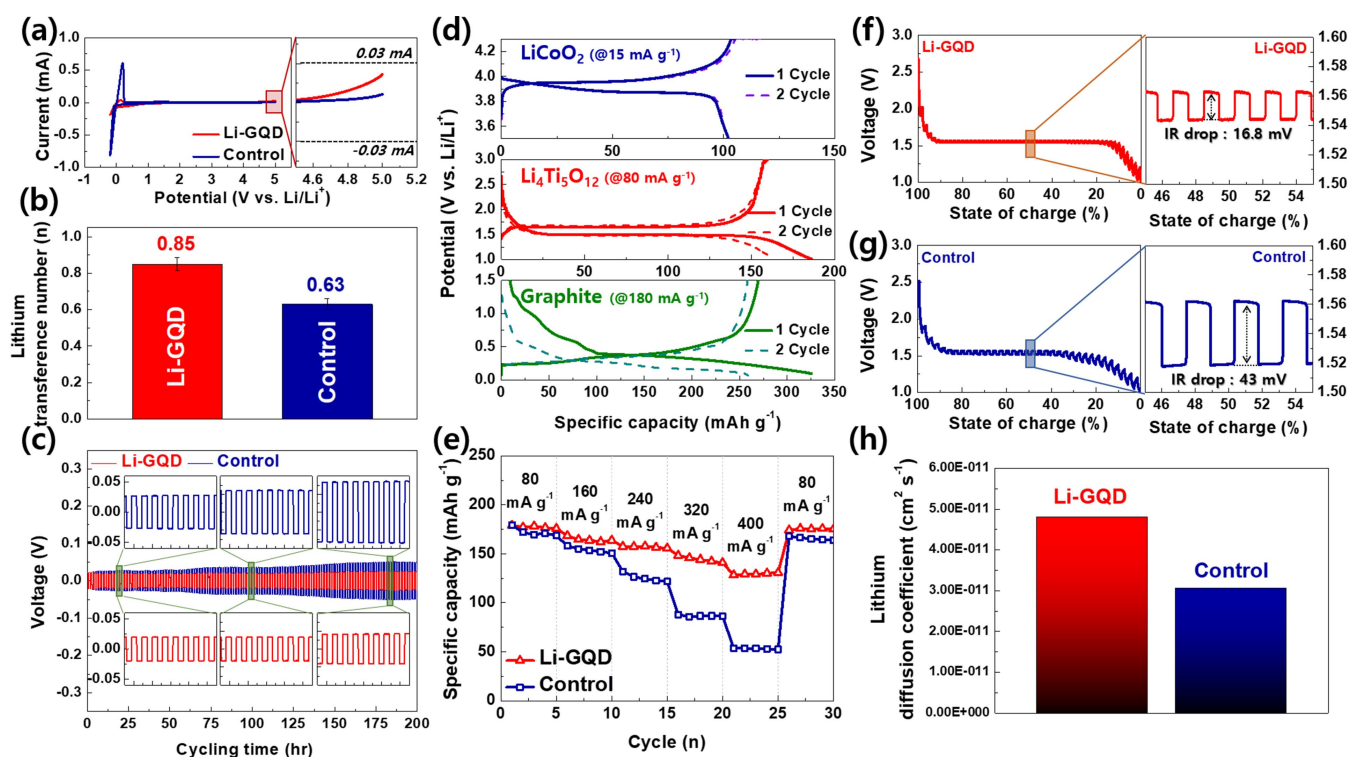


Figure 3. a) The electrochemical stability windows of Li-GQD (red line) and the control (blue line) on non-active electrodes. Measurements were performed on Pt disk as working electrodes between –0.2 and 5.0 V vs. Li/Li⁺ at 10 mV s⁻¹. b) The lithium transference numbers of Li-GQD and control. c) The voltage profiles of the samples for lithium stripping and plating tests in a symmetric Li/Li coin cell at a current density of 0.1 mA cm⁻² at 30 °C. d) Coin cell performances using three representative electrode materials: graphite, Li₄Ti₅O₁₂ (LTO), and LiCoO₂ (LCO). e) Capacity versus cycle number of samples using LTO at 80, 160, 240, 320, and 400 mA g⁻¹. The galvanostatic intermittent titration technique (GITT) analysis of f) Li-GQD and g) control. h) The lithium diffusion coefficient of Li-GQD and control calculated from GITT analysis.

that the Li-GQD electrolyte can be successfully applied to various types of LIBs. In Figure 3(d), the LCO and the LTO half-cell showed the plateau region between 3.84–4.09 V and 1.49–1.65 V, respectively, in the charge/discharge curve of the first cycle. In the case of graphite, the plateau region in the 0.7–1.0 V observed in the charge/discharge curve of the graphite half-cell indicates the formation of the SEI film, and the plateau region that appears below 0.3 V is due to insertion/desertion of Li^+ cations.^[50–52] Figure 3(e) shows that the Li-GQD electrolyte provided superior capacity over Control of the same concentration in all current density (80–400 mAg⁻¹) regions in the LTO half cell. In particular, at 400 mAg⁻¹, the highest current density, the capacity of the Li-GQD electrolyte was about 2.4 times higher than that of Control. Overvoltage was also significantly lower during the charging/discharging process in the Li-GQD electrolyte (Figure S6). Overall, Li-GQD is inferred to provide more free Li^+ than LiPF₆ of the same concentration, thereby reducing the concentration polarization of Li^+ cations at the electrode-electrolyte interface during the charging/discharging process, which presumably allows the superior battery performance.

In the galvanostatic intermittent titration technique (GITT) analysis, IR-drop in the Li-GQD electrolyte was 16.8 mV during the 10 min discharging/relaxation cycles, which is 60.9% smaller than Control (43.1 mV) (Figure 3f and g). The Li^+ diffusion coefficient (D) was calculated using the following Equation (2):

$$D = \frac{4}{\pi\tau} \left(\frac{n_m V_m}{S} \right)^2 \left(\frac{\Delta E_s}{\Delta E_t} \right)^2, \quad (2)$$

where τ is the current pulse time (s), n_m is the number of moles of Li^+ cations in the electrode (mol); V_m is the molar volume of electrode (cm³ mol⁻¹), S is the electrode/electrolyte contact area (cm²), ΔE_s is the steady-state voltage change due to the current

pulse, and ΔE_t is the voltage change during the constant current pulse. In Figure 3(h), D of the Li-GQD electrolyte showed an improved value by 57.3% (4.80×10^{-11} cm² s⁻¹) over control (3.05×10^{-11} cm² s⁻¹). As a result, the Li-GQD electrolyte showed significant electrochemical stability, Li^+ -dynamic properties, and battery performance despite insufficient solubility in organic solvents. Li-GQD possesses considerable potential as an electrolyte composition in LIBs and is expected to secure improved electrochemical performance in future research.

Electrochromic performance of PB in the K-GQD aqueous electrolyte

One of the essential properties required as an electrolyte is the electrochemical inertness of its anion in dissolved states.^[53] For example, the electrolytes mainly used in rechargeable Mg batteries are Mg-containing chloride complexes, and the strong corrosivity of Cl⁻ has been the main obstacle in their performance improvement.^[54] PB, the representative active material in the electrochromic device, is known to be sensitive to the type of the electrolyte anion and readily degraded under Cl⁻ or CO₃²⁻ anionic condition during the redox process.^[55] We investigated the electrochemical behaviour of the PB thin film under various electrolyte conditions, including K-GQD and commercially available control groups such as KCl, K₂CO₃, and K₂SO₄ in aqueous conditions. The PB thin film showed reversible oxidation/reduction behavior at around 0.21 V in a K-GQD solution (Figure 4a). The EIS spectra in Figure 4b showed the interfacial charge transfer resistance ($R_{ct} = 53 \Omega$) is significantly lower in the K-GQD based electrolyte than the other electrolyte during the redox process of the PB thin film (80–214 Ω). The redox reaction of the PB thin film relies on the insertion and desertion process of K⁺ cations, which are the

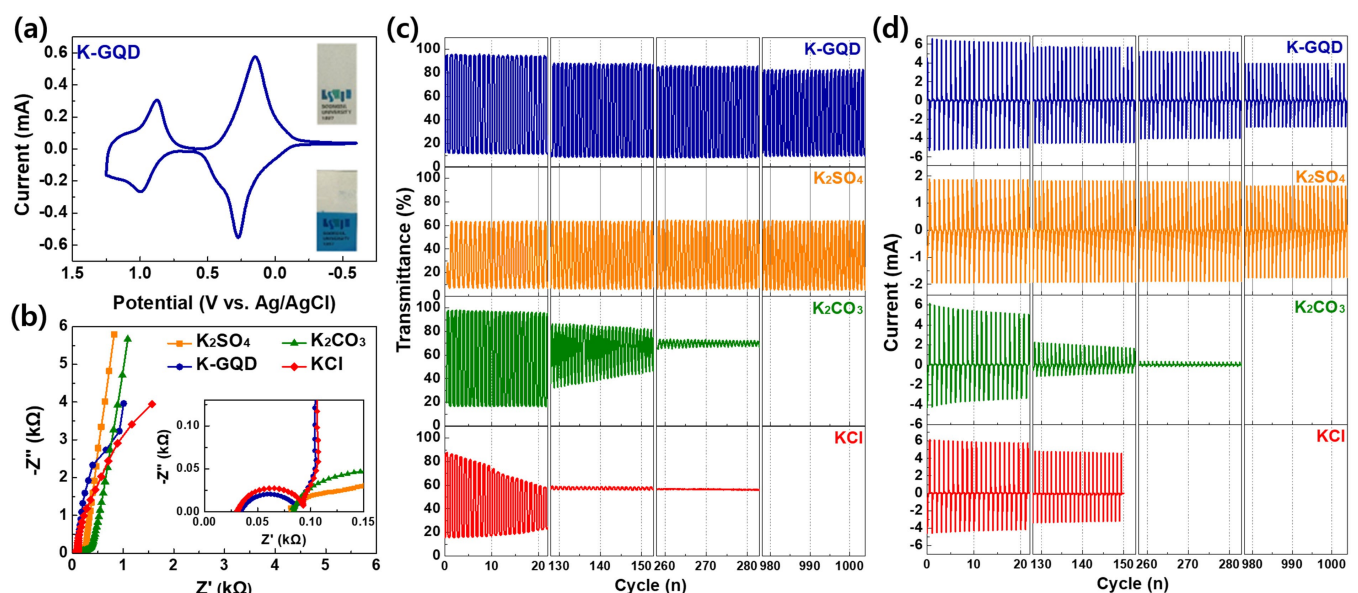


Figure 4. a) Cyclic voltammograms of PB thin films in 0.5 M K-GQD under three-electrode system. b) Electrochemical impedance spectra (EIS) of PB thin films under ac amplitude of 5 mV. c, d) in situ optical transmittance and current change of PB thin films under K-GQD, K₂SO₄, K₂CO₃, and KCl, respectively.

rate determination steps of the entire charge-transfer kinetics.^[56] Thus, the lower R_{ct} under the K-GQD electrolyte means that K-GQD provides the higher K^+ cation transport than other common salts in aqueous conditions, which corresponds with the earlier MD simulation and battery study. Low R_{ct} promotes the improved switching time and stable electrochromic performance of the PB thin film.^[57]

The electrochromic properties of the PB thin film were then explored in a three-electrode system. The colouration efficiency (η), one of the critical parameters, is calculated as Equation (3).^[58]

$$\eta(\lambda) = \frac{\Delta OD}{\Delta Q} = \frac{\log\left(\frac{T_b}{T_c}\right)}{\Delta Q}, \quad (3)$$

where OD is the logarithm of the ratio between the transmittance at the bleaching and colouration states. T_c and T_b refer to transmittance reaching 10% and 90% of its full modulation, respectively, at 700 nm absorbance. The measured parameter values for each electrolyte were summarized in Table S2. When under the K-GQD electrolyte, the PB thin film showed higher η ($103.0 \text{ cm}^2 \text{ C}^{-1}$) and ΔOD (0.89), faster color switching (t_b , bleaching time = 1.5 and t_c , coloring time = 2.1 s) than KCl and K_2CO_3 . Note that the PB thin films using KCl and K_2CO_3 exhibited significant degradation of electrochromism after 130 and 260 operation cycles, respectively (Figure 4c and d). It is known that the lattice defect sites (vacant sites) of $Fe^{III}_4[Fe^{II}(CN)_6]_3$, in the face-centred cubic (FCC) structure of PB, are chemically attacked by Cl^- and CO_3^{2-} anions, causing the decomposition and undesired side reaction of PB.^[59] In contrast, K-GQD was expected to allow stable electrochromic performance as the hydrated size of the GQD polyanion is too large to enter inside the PB lattice (<5.1 Å). In Figure 4(c, d), K-GQD exhibited only ~3% degradation in ΔT from the initial operating cycle to 1000 times. Furthermore, the PB thin films under K-GQD showed about 3.2 times faster switching in colour change and about 42% higher ΔT than K_2SO_4 .

Conclusion

We demonstrate a new class of electrolyte salts, including the nano-sized GQD polyanions and alkali metal cations. The synthesized ionic salts readily dissolve in protic solvent providing excellent cation mobility and ionic conductivity. A nano-sized, chemically inert, carbonized structure of the GQD polyanion meets some of the requirements for weakly coordinated anions resulting in a high dissociation rate and transport number of counter cations in dissolved electrolytes. Li-GQD used in the LIB application exhibits higher interfacial stability at the Li metal anode than conventionally used $LiPF_6$ and offers a wide electrochemical stability window to multiple electrode materials. Just with the feasibility tests, the Li-GQD electrolyte shows a more favourable electrochemical kinetic parameter, including a lower IR drop (16.8 mV) and a higher lithium

diffusion coefficient ($4.80 \times 10^{-11} \text{ cm}^2 \text{ s}^{-1}$) than $LiPF_6$. As the aqueous electrolyte, the K-GQD electrolyte provides the high K^+ cation transfer to the PB thin film, allowing superior electrochromic performance, including excellent colouration efficiency (η , $103.0 \text{ cm}^2 \text{ C}^{-1}$), high optical contrast (ΔOD , 0.89), and fast colour switching (t_b , bleaching time = 1.5 and t_c , colouring time = 2.1 s) over conventional electrolytes. Long-term stability performance is achieved due to the chemical inertness of the GQD polyanion, unlike other anions Cl^- , CO_3^{2-} , and SO_4^{2-} . We expect our new class of ionic salts to be another signpost for exploring innovative electrolyte systems for next-generation electrochemical devices.

Supporting Information

Supporting Information is available from the Wiley Online Library or from the author.

Acknowledgements

This work was supported by the research grants from National Research Foundation of Korea (2017M3A9D8029943, 2018R1D1A1B05050938, 2019M3E6A1104186, 2020R1A2C2010510), Korea Institute of Science and Technology Information (KSC-2020-CRE-0224), and Technology development Program of MSS (S2974093).

Conflict of Interest

The authors declare no conflict of interest.

Data Availability Statement

The data that support the findings of this study are available in the supplementary material of this article.

Keywords: electrochromic device • electrolyte salt • graphene quantum dot • ionic compound • lithium-ion battery

- [1] R. H. Stokes, R. A. Robinson, *J. Am. Chem. Soc.* **1948**, *70*, 1870–1878.
- [2] S. Zhang, Y. Ki, H. Song, X. Chen, J. Zhou, S. Hong, M. Huang, *Sci. Rep.* **2016**, *6*, 19292.
- [3] C. Zhong, Y. Deng, W. Hu, J. Qiao, L. Zhang, J. Zhang, *Chem. Soc. Rev.* **2015**, *44*, 7484–7539.
- [4] A. Ziombor, A. Machnik, A. Dahlmann, P. Dietsch, F.-X. Beck, H. Wagner, K. F. Hilgers, F. C. Luft, K.-U. Eckardt, J. Titze, *Am. J. Physiol. Ren. Physiol.* **2008**, *295*, F1752–F1763.
- [5] D. N. Müller, N. Wilck, S. Haase, M. Kleinewietfeld, R. A. Linker, *Nat. Rev. Immunol.* **2019**, *19*, 243–254.
- [6] M. P. Blaustein, F. H. H. Leenen, L. Chen, V. A. Golovina, J. M. Hamlyn, T. L. Pallone, J. W. v. Huysse, J. Zhang, W. G. Wier, *Am. J. Physiol. Heart Circ. Physiol.* **2012**, *302*, H1031–H1049.
- [7] B. J. Kinsman, K. N. Browning, S. D. Stocker, *J. Physiol.* **2017**, *595*, 6187–6201.
- [8] S. Clark, A. Latz, B. Horstmann, *ChemSusChem* **2017**, *10*, 4735–4747.

- [9] X. Yu, Y. Fu, X. Cai, H. Kafafy, H. Wu, M. Peng, S. Hou, Z. Lv, S. Ye, D. Zou, *Nano Energy* **2013**, *2*, 1242–1248.
- [10] Z. Zeng, V. Murugesan, K. S. Han, X. Jiang, Y. Cao, L. Xiao, X. Ai, H. Yang, J.-G. Zhang, M. L. Sushko, J. Liu, *Nat. Energy* **2018**, *3*, 674–681.
- [11] B. C. H. Steele, A. Heinzel, *Nature* **2001**, *414*, 345–352.
- [12] L. Xiao, S. Zhang, J. Pan, C. Yang, M. He, L. Zhuang, J. Lu, *Energy Environ. Sci.* **2012**, *5*, 7869–7871.
- [13] Q. Zhao, X. Liu, S. Stalin, K. Khan, L. A. Archer, *Nat. Energy* **2019**, *4*, 365–373.
- [14] M. D. Tikekar, S. Choudhury, Z. Tu, L. A. Archer, *Nat. Energy* **2016**, *1*, 16114.
- [15] R. D. Rogers, K. R. Sedden, *Science* **2003**, *302*, 792–793.
- [16] X. Li, J. Liang, X. Yang, K. R. Adair, C. Wang, F. Zhao, X. Sun, *Energy Environ. Sci.* **2020**, *13*, 1429–1461.
- [17] H. Wu, Y. Xu, X. Ren, B. Liu, M. H. Engelhard, M. S. Ding, P. Z. El-Khoury, L. Zhang, Q. Li, K. Xu, C. Wang, J.-G. Zhang, W. Xu, *Adv. Energy Mater.* **2019**, *9*, 1902108.
- [18] J. C. Bachman, S. Muy, A. Grimaud, H.-H. Chang, N. Pour, S. F. Lux, O. Paschos, F. Maglia, S. Lupart, P. Lamp, L. Giordano, Y. Shao-Horn, *Chem. Rev.* **2016**, *116*, 140–162.
- [19] S. Hu, A. Trinchi, P. Atkin, I. Cole, *Angew. Chem. Int. Ed.* **2015**, *54*, 2970–2974; *Angew. Chem.* **2015**, *127*, 3013–3017.
- [20] X. Zhang, Y. Zhang, Y. Wang, S. Kalytchuk, S. V. Kershaw, Y. Wang, P. Wang, T. Zhang, Y. Zhao, H. Zhang, T. Cui, Y. Wang, J. Zhao, W. W. Yu, A. L. Rogach, *ACS Nano* **2013**, *7*, 11234–11241.
- [21] F. Yuan, S. Li, Z. Fan, X. Meng, L. Fan, S. Yang, *Nano Today* **2016**, *11*, 565–586.
- [22] H. C. Lim, S. H. Min, E. Lee, J. Jang, S. H. Kim, J.-I. Hong, *ACS Appl. Mater. Interfaces* **2015**, *7*, 11069–11073.
- [23] E. Lee, J. Ryu, J. Jang, *Chem. Commun.* **2013**, *49*, 9995.
- [24] X. T. Zheng, A. Ananthanarayanan, K. Q. Luo, P. Chen, *Small* **2015**, *11*, 1620–1636.
- [25] S. Mondal, A. Yucknovsky, K. Akulov, N. Ghorai, T. Schwartz, H. N. Ghosh, N. Amdursky, *J. Am. Chem. Soc.* **2019**, *141*, 15413–15422.
- [26] D. Pan, J. Zhang, Z. Li, M. Wu, *Adv. Mater.* **2010**, *22*, 734–738.
- [27] F. Liu, M.-H. Jang, H. D. Ha, J.-H. Kim, Y.-H. Cho, T. S. Seo, *Adv. Mater.* **2013**, *25*, 3657–3662.
- [28] Z. Li, W. Zhang, J. Yang, J. G. Hou, *J. Am. Chem. Soc.* **2009**, *131*, 6320–6321.
- [29] A. C. Ferrari, J. C. Meyer, V. Scardaci, C. Casiraghi, M. Lazzeri, F. Mauri, S. Pisacane, D. Jiang, K. S. Novoselov, S. Roth, A. K. Geim, *Phys. Rev. Lett.* **2006**, *97*, 187401.
- [30] I. Lorite, A. del Campo, J. J. Romero, J. F. Fernández, *J. Raman Spectrosc.* **2012**, *43*, 889–894.
- [31] K. Yang, K. Cho, D. S. Yoon, S. Kim, *Sci. Rep.* **2017**, *7*, 40163.
- [32] . Peng, M. Gobet, M. Devany, K. Xu, A. v. W. Cresce, O. Borodin, S. Greenbaum, J. Power Sources **2018**, *399*, 215–222.
- [33] O. Borodin, G. D. Smith, *J. Phys. Chem. B* **2009**, *113*, 1763–1776.
- [34] M. P. Allen, D. J. Tildesley, *Computer Simulation of Liquids*, Oxford University Press, New York, USA **1987**.
- [35] P. Atkins, J. de Paula, *Physical Chemistry 8ed*, W. H. Fredman, New York, USA **2006**.
- [36] R. J. LeSuer, C. Buttolph, W. E. Geiger, *Anal. Chem.* **2004**, *76*, 6395–6401.
- [37] M. S. Ding, T. R. Jow, *J. Electrochem. Soc.* **2004**, *151*, A2007–A2015.
- [38] Y. Marcus, *Chem. Rev.* **1988**, *88*, 1475–1498.
- [39] S. H. Strauss, *Chem. Rev.* **1993**, *93*, 927–942.
- [40] I. Krossing, I. Raade, *Chem. Eur. J.* **2004**, *10*, 5017–5030.
- [41] H. Zhang, H. Han, X. Cheng, X. Cheng, L. Zheng, P. Cheng, W. Feng, J. Nie, M. Armand, X. Huang, Z. Zhou, *J. Power Sources* **2015**, *296*, 142–149.
- [42] I. M. Riddlestone, A. Kraft, J. Schaefer, I. Korssing, *Angew. Chem. Int. Ed.* **2017**, *57*, 13982–14024.
- [43] P. Murmann, P. Niehoff, R. Schmitz, S. Nowak, H. Gores, N. Ignatiev, P. Sartori, M. Winter, R. Schmitz, *Electrochim. Acta* **2013**, *114*, 658–666.
- [44] Y. Huang, Z. Liang, H. Wang, *Chem. Commun.* **2020**, *56*, 10070–10073.
- [45] Y. Huang, L. Qi, H. Wang, *Electrochim. Acta* **2017**, *258*, 380–387.
- [46] H. Zhang, C. Li, M. Piszzcz, E. Coya, T. Rojo, L. M. Rodriguez-Martinez, M. Armand, Z. Zhou, *Chem. Soc. Rev.* **2017**, *46*, 797–815.
- [47] Y. Lu, M. Tikekar, R. Mohanty, K. Hendrickson, L. Ma, L. A. Archer, *Adv. Energy Mater.* **2015**, *5*, 1402073.
- [48] Z. Jin, K. Xie, X. Hong, *J. Mater. Chem. A* **2013**, *1*, 342–347.
- [49] J. L. Schaefer, D. A. Yanga, L. A. Archer, *Chem. Mater.* **2013**, *25*, 834–839.
- [50] Y. Kim, H. Seo, E. Kim, I. Seo, *Nanomaterials* **2020**, *10*, 1705.
- [51] L. Gan, H. Guo, Z. Wang, X. Li, W. Peng, J. Wang, S. Huang, M. Su, *Electrochim. Acta* **2013**, *104*, 117–123.
- [52] R. Makirua, S. Teragawa, K. Tsuchiyama, M. Tatsumisago, *Dalton Trans.* **2015**, *44*, 15279–15285.
- [53] J. Luo, Y. Bi, L. Zhang, X. Zhang, T. L. Liu, *Angew. Chem. Int. Ed. Engl.* **2019**, *58*, 6967–6971.
- [54] S. He, K. V. Nielson, J. Luo, T. L. Liu, *Energy Storage Mater.* **2017**, *8*, 184–188.
- [55] A. Roig, J. Navarro, R. Tamarit, F. Vicente, *J. Electroanal. Chem.* **1993**, *360*, 55–69.
- [56] D. R. Rosseinsky, L. Glasser, H. D. B. Jenkins, *J. Am. Chem. Soc.* **2004**, *126*, 10472–10477.
- [57] N. S. Pham, Y. H. Seo, E. Park, Y. D. D. Nguyen, I.-S. Shin, *Electrochim. Acta* **2020**, *353*, 136446.
- [58] J.-F. Feng, T.-F. Liu, R. Cao, *Angew. Chem. Int. Ed.* **2020**, *59*, 22392–22396; *Angew. Chem.* **2020**, *132*, 22578–22582.
- [59] J. Agrisuelas, J. J. García-Jareño, F. Vincente, *J. Phys. Chem. C* **2012**, *116*, 1935–1947.
- [60] K. Vanommeslaeghe, E. Hatcher, C. Acharya, S. Kundu, S. Zhong, J. Shim, E. Darian, O. Guvench, P. Lopes, I. Vorobyov, A. D. Mackerell Jr, *J. Comput. Chem.* **2010**, *31*, 671–690.
- [61] B. R. Brooks, C. L. Brooks III, A. D. Mackerell Jr, L. Nilsson, R. J. Petrella, B. Roux, Y. Won, G. Archontis, C. Bartels, S. Boresch, A. Cafisch, L. Caves, Q. Cui, A. R. Dinner, M. Feig, S. Fischer, J. Gao, M. Hodoscek, W. Im, K. Kuczera, T. Lazaridis, J. Ma, V. Ovchinnikov, E. Paci, R. W. Pastor, C. B. Post, J. Z. Pu, M. Schaefer, B. Tidor, R. M. Venable, H. L. Woodcock, X. Wu, W. Yang, D. M. York, M. Karplus, *J. Comput. Chem.* **2009**, *30*, 1545–1614.
- [62] H. C. Andersen, *J. Chem. Phys.* **1980**, *72*, 2384.
- [63] G. J. Martyna, D. J. Tobias, M. L. Klein, *J. Chem. Phys.* **1994**, *101*, 4177.
- [64] W. G. Hoover, *Phys. Rev. A* **1985**, *31*, 1695.
- [65] T. Darden, D. York, L. Pedersen, *J. Chem. Phys.* **1993**, *98*, 10089.
- [66] G. M. Torrie, J. P. Valleau, *Chem. Phys. Lett.* **1974**, *28*, 578–690.
- [67] G. M. Torrie, J. P. Valleau, *J. Comput. Phys.* **1977**, *23*, 187–199.
- [68] S. Kumar, J. M. Rosenberg, D. Bouzida, R. H. Swendsen, P. A. Kollman, *J. Comput. Chem.* **1992**, *13*, 1011–1021.
- [69] M. Souaille, B. Roux, *Comput. Phys. Commun.* **2001**, *135*, 40–57.

Manuscript received: November 22, 2021
Revised manuscript received: December 7, 2021
Accepted manuscript online: December 8, 2021
Version of record online: December 23, 2021